

## Supporting Information

### **More Than 12 % Polarization and 20 Minute Lifetime of $^{15}\text{N}$ on Choline Derivative Utilizing Parahydrogen and a Rhodium Nanocatalyst in Water**

*Jeffrey McCormick, Sergey Korchak, Salvatore Mamone, Yavuz N. Ertas, Zhiyu Liu, Luke Verlinsky, Shawn Wagner, Stefan Glögger,\* and Louis-S. Bouchard\**

anie\_201804185\_sm\_miscellaneous\_information.pdf

# Supporting Information

<b>S1</b> Materials and General Methods	2
<b>S2</b> Synthesis Procedure	3
<b>S3</b> Nanoparticle Characterization	4
<b>S4</b> Parahydrogen-Induced Polarization (PHIP) Experiments	8
<b>S5</b> Polarization Calculations	12
<b>S6</b> References	12

# S1 Materials and Methods

## Chemicals and Supplies

Rhodium chloride hydrate, 99% ( $\text{RhCl}_3 \cdot x\text{H}_2\text{O}$ ), sodium borohydride ( $\text{NaBH}_4$ ), N-acetylcysteine (NAC), 1- $^{13}\text{C}$ -hydroxyethyl acetate- $d_3$  (HEA), vinyl acetate, and  $d_{12}$ - $^{15}\text{N}$ -trimethylvinylammonium hydroxide (neurine) were purchased from Sigma Aldrich and used without further modification. Solvents for purification such as *n*-hexanes, anhydrous isopropanol and anhydrous, absolute ethanol were purchased from Fisher Scientific and used as received, unless degassed by repeated freeze-pump-thaw cycles. MilliQ water was generated by in house filtration and collected at  $\geq 17.9 \text{ M}\Omega$  resistance. Deuterated solvents ( $\text{D}_2\text{O}$  and  $\text{CDCl}_3$ ) were purchased by Cambridge Isotope Laboratories and used as received. Degassed solvents were prepared by no less than three freeze-pump-thaw cycles of submerging in liquid nitrogen, pulling static vacuum for  $\sim 30$  minutes, and slowly thawing in a water bath before allowing nitrogen flow. Parahydrogen was enriched to  $\sim 90\%$  by a Bruker BPHG-90 parahydrogen generator and used in continuous flow mode for high field experiments (neurine and HEA) or by a generator from Advanced Research Systems, Inc. (DE202AI) stored in compressed cylinders for earth field experiments (vinyl acetate, VA).

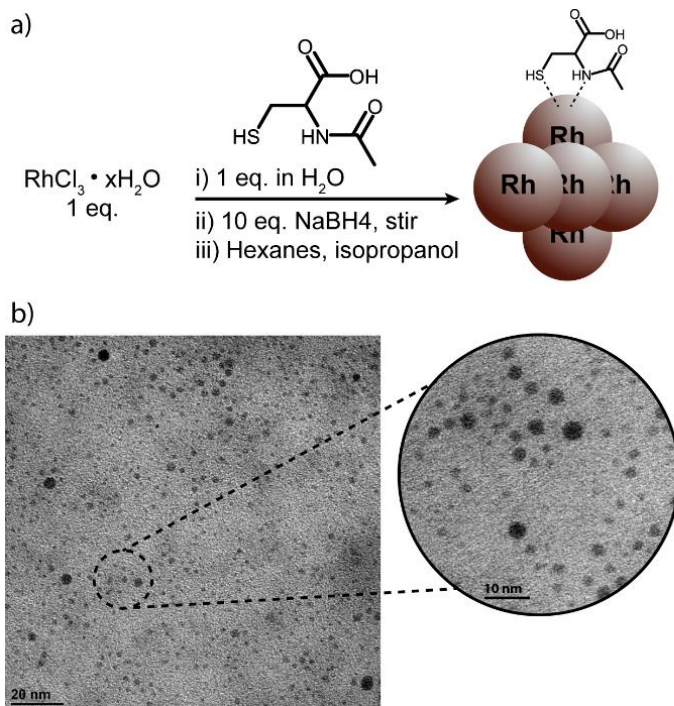
## Nanoparticle and Ligand Characterization

NMR measurements were recorded on a Bruker AV300 system using a 5 mm broadband probe for high field PASADENA PHIP experiments (HEA and neurine) as well as all  $^1\text{H}$  and  $^{13}\text{C}$   $T_1$  measurements. A Bruker AV600 system with a broadband probe was used to measure the ALTADENA and field cycling experiments of VA, as well as the  $T_1$  value of  $^{15}\text{N}$  on NETMA. Thermogravimetric analysis (TGA) of nanoparticle ligand coverage was measured using a Perkin Elmer Pyris Diamond TG/DTA in alumina pans spanning from  $30^\circ\text{C}$  to  $825^\circ\text{C}$  under argon flow at  $5^\circ\text{C}/\text{min}$ . Transmission electron microscopy was performed using an FEI Tecnai T12 microscope after suspension of nanoparticles in MilliQ water and drying on carbon substrate grids treated with plasma cleaning for 20 seconds before preparation. X-ray photoemission spectroscopy (XPS) studies were carried out on a Kratos AXIS Ultra DLD X-ray photoelectron spectrometer with a monochromatic Al  $K\alpha$  X-ray source operating at 10 mA and 15 kV. Centrifugation was performed on a Beckman Avanti J-25 using a JA-14 rotor. Inert chemistry was conducted using standard Schlenk technique under nitrogen flow.

## S2 Synthesis Procedure

### Synthesis of N-acetylcysteine-Capped Rhodium Nanoparticles (NAC@Rh)

Inert synthesis conditions were modified from previously published work<sup>[1]</sup>. 209 mg of  $\text{RhCl}_3$  (1 mmol) was added to a 500 mL flask under argon atmosphere before addition of 100 mL degassed MilliQ water and stirred at 360 RPM under nitrogen flow to produce 10 mM  $\text{Rh}^{3+}$  precursor solution. In a separate flask, 163 mg N-acetylcysteine (1 mmol) was dissolved in 27.5 mL degassed MilliQ water and added into the  $\text{Rh}^{3+}$  solution quickly. Addition of the ligand solution causes subtle color change from transparent pink to vibrant rose color. After stirring for 1 hour, a fresh solution of 377 mg  $\text{NaBH}_4$  (10 mmol) was prepared in 15 mL degassed MilliQ water, and added to the  $\text{Rh}^{3+}$ :NAC solution dropwise over 4 minutes. Introduction of  $\text{NaBH}_4$  causes immediate color change to black, indicating reduction into nanoparticles. Freshly formed nanoparticles were left to stir overnight before solvent fractionation by addition of 160 mL isopropanol and 53 mL *n*-hexanes for 3 hours stirring at 360 RPM. Solution was balanced and centrifuged at 6000 RPM (5509xg) for 25 minutes, producing an insoluble fraction pellet to be discarded. Supernatants were stirred with an additional 100 mL isopropanol for 3 hours producing desired particle pellet, centrifuged again at 6000 RPM, and supernatants were discarded. Pellet was washed 4x with absolute ethanol before drying under static vacuum prior to use. Particle sizing by TEM indicates an average particle size of  $2.4 \pm 0.4$  nm, and measurements by inductively coupled plasma mass spectrometry (ICP-MS) were unable to detect dissolved Rh ions in the supernatant of centrifuged particles, demonstrating their heterogeneous nature (see S3).



**Scheme 1.** a) Synthesis of NAC@Rh. b) TEM image of NAC@Rh after dispersion in water.

# S3 Nanoparticle Characterization

## Transmission Electron Microscopy (TEM) of NAC@Rh Particles

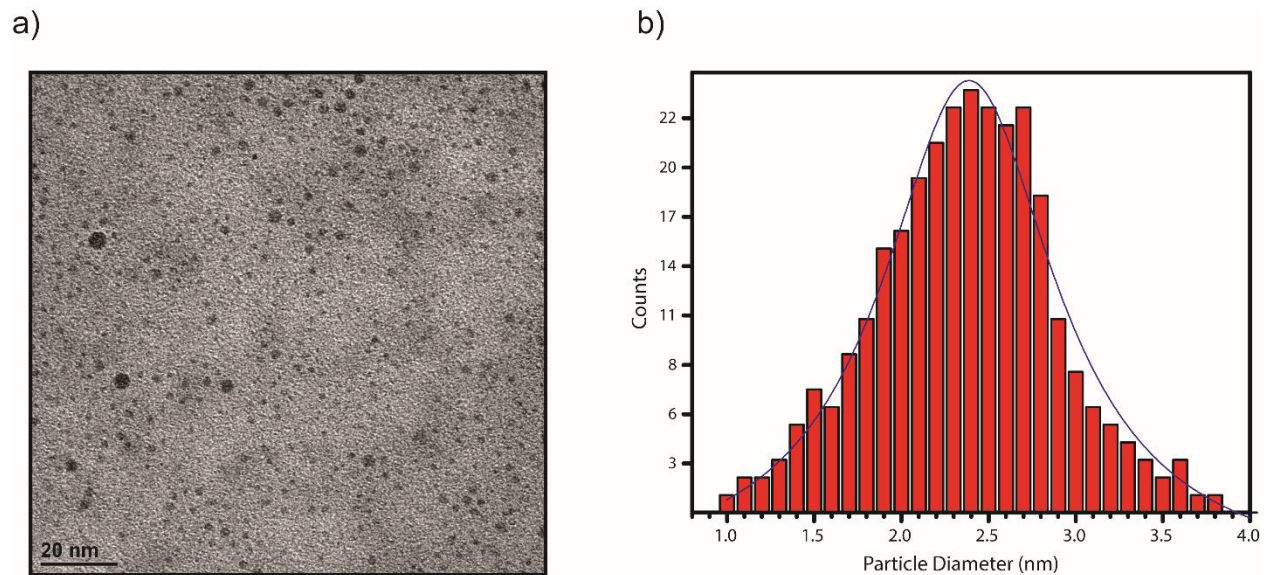


**Figure S3.** a) Image of NAC@Rh particles taken by TEM following dispersion in MilliQ water. b) Plot of particle diameters after counting to determine average particle size.

294 particles of NAC@Rh were chosen at random and compiled into the size distributions shown in Fig S3 a) and b) respectively. An average particle size of  $2.4 \pm 0.4$  nm was determined. Deviations were calculated from the Gaussian fits shown in Fig S3b).

## Thermogravimetric Analysis (TGA)

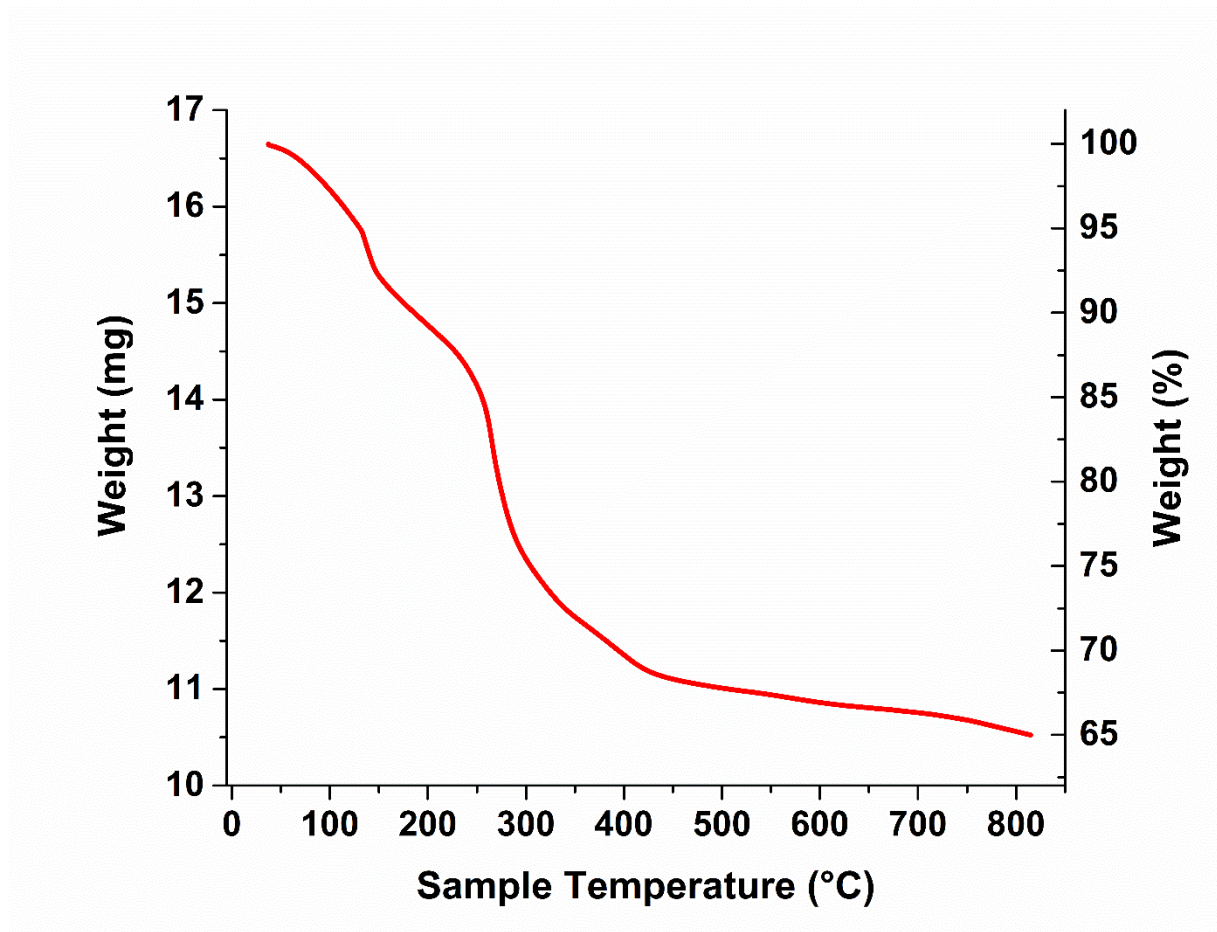


**Figure S4.** Curve showing NAC@Rh mass from 30°C to 825°C at 5°C/min under argon flow. Ligand decomposition reveals a final Rh mass of approximately 65% by sample weight.

### Characterization of Ligand Coordination by NMR

To assess ligand coordination to the Rh surface,  $^1\text{H}$  NMR is used to determine line broadening of NAC caused by dipolar interactions upon coordination with Rh.

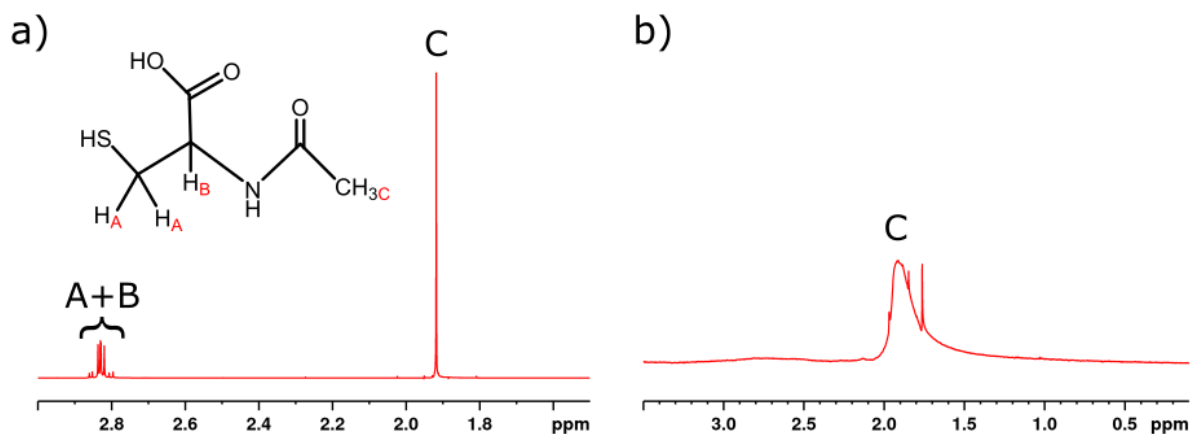


**Figure S5.**  $^1\text{H}$  NMR spectrum of a) NAC only and b) NAC@Rh dispersed in  $\text{D}_2\text{O}$ .

### X-ray Photoelectron Spectroscopy (XPS) of NAC@Rh

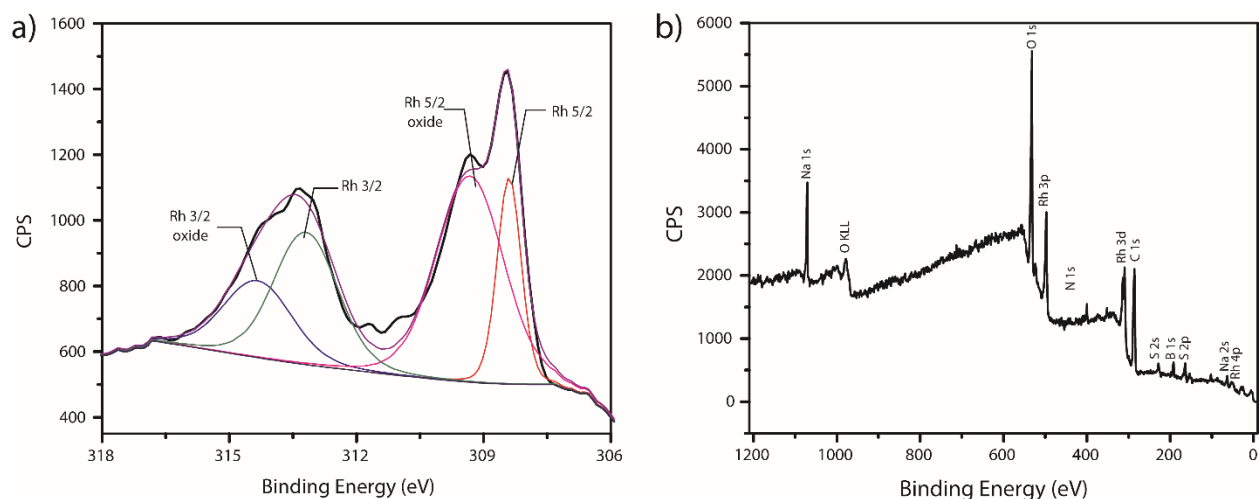


**Figure S6.** a) XPS spectrum showing  $\text{Rh}_{3/2}$  and  $\text{Rh}_{5/2}$  peaks corresponding to metal surface of the NAC@Rh. b) Survey spectrum of NAC@Rh showing contributions of NAC coordinated to the surface.

XPS measurements were performed on a Kratos AXIS Ultra DLD X-ray photoelectron spectrometer with a monochromatic  $\text{Al K}\alpha$  X-ray source operating at 10 mA and 15 kV using the neutralizer. Survey spectra and individual high-resolution spectra were collected using pass energies of 160 eV and 20 eV, respectively. Data processing was performed using CasaXPS 2.3 software, and spectral binding energies were calibrated by assigning the hydrocarbon peak in the C 1s high-resolution spectra, as a result of adventitious carbon, to 284.6 eV. Catalytically active  $\text{Rh}^0$  as well as contributions from ligands such as C, S, O, and N are represented in the survey spectrum (Fig S6b). Rhodium oxide formation present is attributable to air atmosphere during sample preparation.

## **Inductively Coupled Plasma Mass Spectrometry (ICP-MS)**

To confirm that there is no ion shedding during synthesis, inductively coupled plasma mass spectrometry (ICP-MS) analysis was performed to detect Rh content from supernatant. The nanoparticle suspension was prepared at 1 mg/mL in MilliQ water and centrifuged at 516,245xg for 5 hrs. The supernatant of each sample transferred to clean tubes (SC475, Environmental Express) for acid digestion. Digestion was carried out with a mixture of concentrated HNO<sub>3</sub> (65-70%, Trace Metal Grade, Fisher Scientific) and HCl (35-38%, Trace Metal Grade, Fisher Scientific) in a ratio of 1:3 with a supplement of H<sub>2</sub>O<sub>2</sub> (30%, Certified ACS, Fisher Scientific) at 95 °C for 6 hrs in a HotBlock (SC100, Environmental Express). Once the sample was cooled to room temperature, it subsequently diluted to make a final volume of 50 mL by adding filtered DI water. DI water in the absence of NAC@Rh was also digested for reagent blank. The Rh content was quantified using an ICP-MS (NexION 2000, PerkinElmer, USA) and a calibration curve was established using a standard Rh solution (AccuStandard, 10 µg/mL in 10 % HCl). Each sample and standard was analyzed in triplicate with background correction.

## **Turnover Frequency (TOF) Measurements**

TOF measurements were performed for each contrast agent investigated. Solutions of NAC@Rh and relevant substrates were prepared and conversion was monitored by <sup>1</sup>H NMR while bubbling H<sub>2</sub> at 80°C under ambient pressure N<sub>2</sub>, which can be considered less aggressive conditions than 6.5 bar H<sub>2</sub> at 90°C during PHIP investigations. Since Rh crystallizes in a face-centered cubic (fcc) arrangement<sup>[2]</sup> and TEM images confirm a nearly spherical geometry, a cubo-octahedral structure can be used in TOF determinations<sup>[3]</sup>. TOFs displayed in Table 1 for HEP shows 1.67-fold and 3.31-fold improvement over previous NAC@Pd and LCys@Pd catalyst systems respectively under identical experimental conditions<sup>[1]</sup>. This also represents the ability to generate 5.52 mM of HEP, 3.44 mM NETMA and 3.94 mM ethyl acetate in the 15s required to hydrogenate using a small parahydrogen volume in an NMR tube and apply transfer polarization methodologies.

# S4 Parahydrogen-Induced Polarization (PHIP) and $T_1$ Measurements

## Experimental Procedure

High field experiments were performed in a Bruker AV300 NMR Spectrometer. NAC@Rh particles were suspended in  $D_2O$  at 0.5 mg/mL along with precursor compounds (HEA and neurine) at 1 mM and degassed prior to experiments by  $N_2$  bubbling. Samples were then pressurized with  $N_2$  to 6 bar while equilibrating to  $80^\circ C$  inside the magnet. Para- $H_2$  was then bubbled through samples at 6.5 bar for 12 seconds achieving full conversion before appropriate pulses were applied. Comparison of hyperpolarized integrals are then compared to standards (1- $^{13}C$ -pyruvate and  $^{15}N$ -urea) and signal enhancements are calculated (see S5). For VA, NAC@Rh and 1 mM VA were added to  $D_2O$  in a J-Young tube under  $N_2$  and heated to  $80^\circ C$  before pressurizing to 5.5 bar with para- $H_2$ . Hydrogenation is initiated by manual shaking under ALTADENA conditions and transporting in and out of a  $\mu$ -metal shield as reported previously<sup>[1]</sup>. Samples were then inserted into a Bruker AV600 NMR Spectrometer and  $^{13}C$  is detected with a single proton-decoupled  $90^\circ$  pulse. Integrals between hyperpolarized product species and thermal spectra are then compared and signal enhancements are calculated. Natural abundance  $^{13}C$  spectra of the EA product were acquired following a  $90^\circ$  pulse, 512 scans with a waiting time of  $5 \times T_1$ . For  $^1H$  polarization, a single  $45^\circ$  scan following bubbling of para- $H_2$  is compared to thermal scans waiting  $5 \times T_1$ .

## $^1H$ NMR Spectra

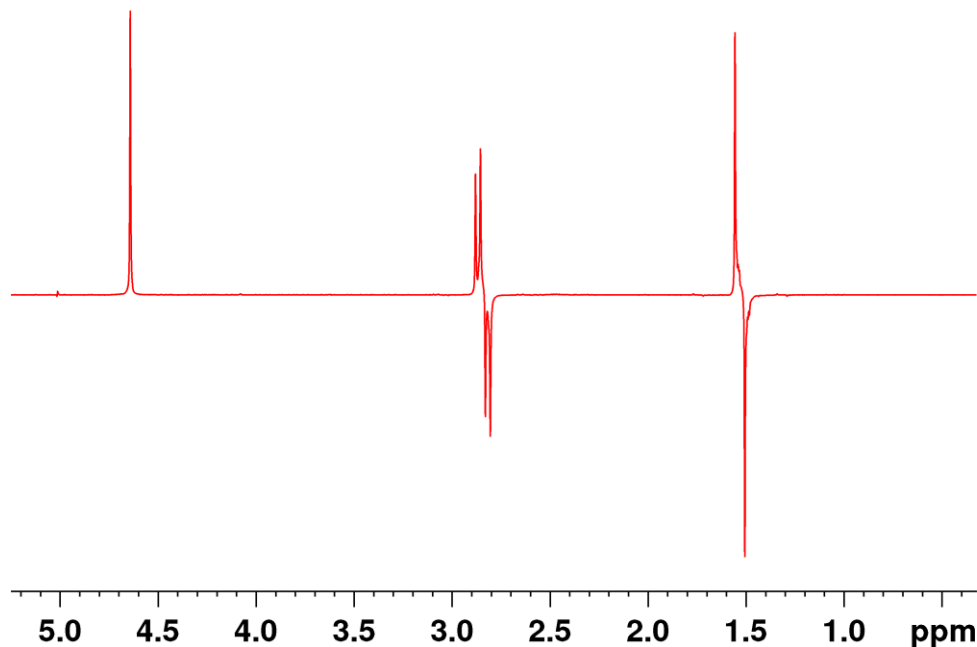


Figure S7.  $^1H$  spectrum of a single scan of HEP formation after para- $H_2$  bubbling.

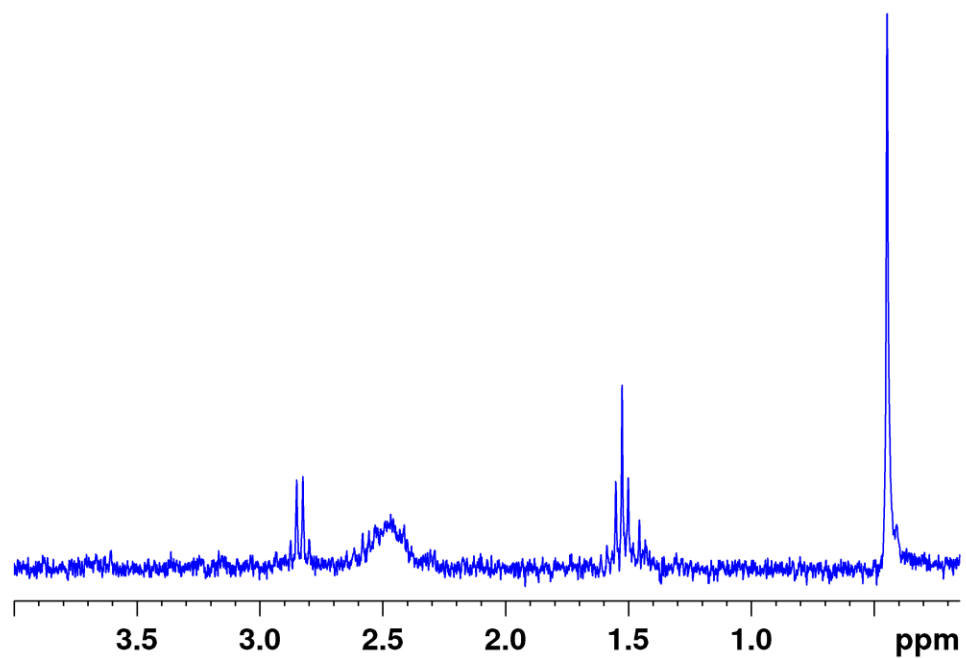


Figure S8. <sup>1</sup>H spectrum of HEP formation after reaching thermal equilibrium after 16 scans.

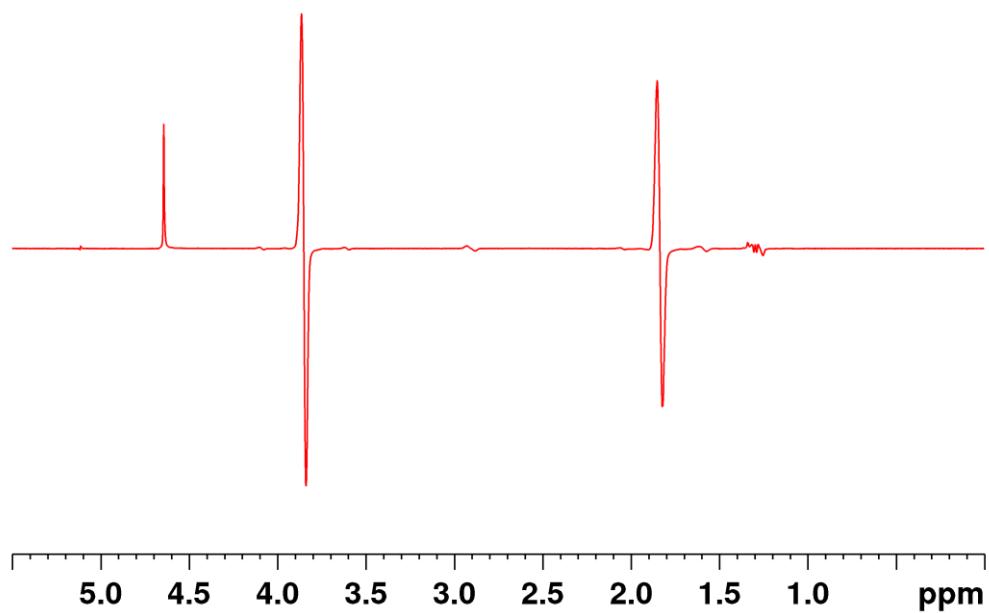


Figure S9. <sup>1</sup>H spectrum of a single scan of NETMA formation after para-H<sub>2</sub> bubbling.

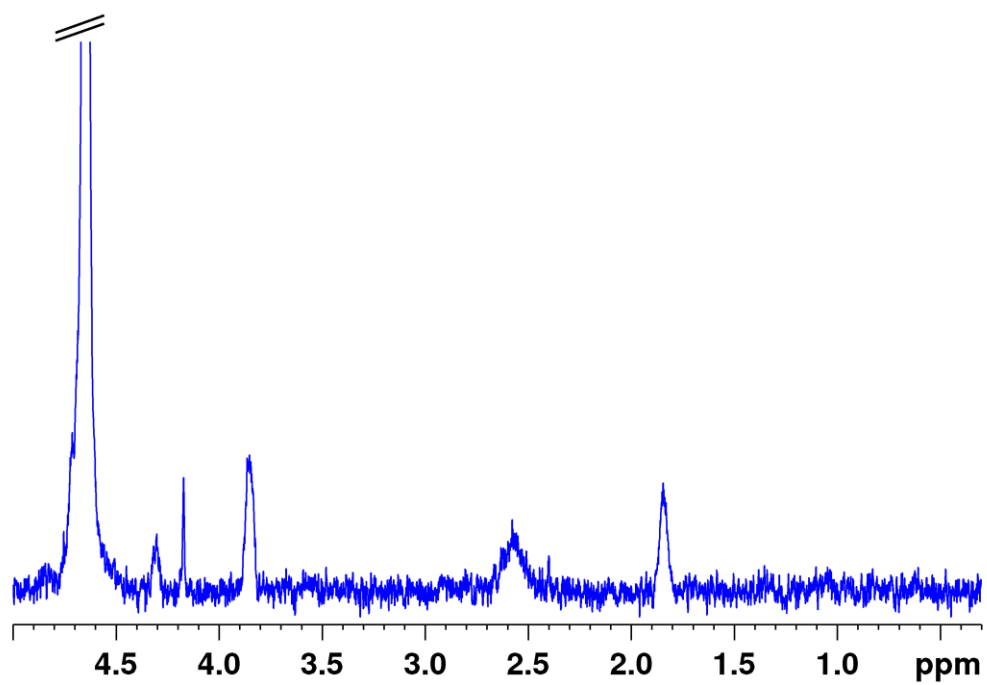


Figure S10. <sup>1</sup>H spectrum of a single scan of NETMA after reaching thermal equilibrium.

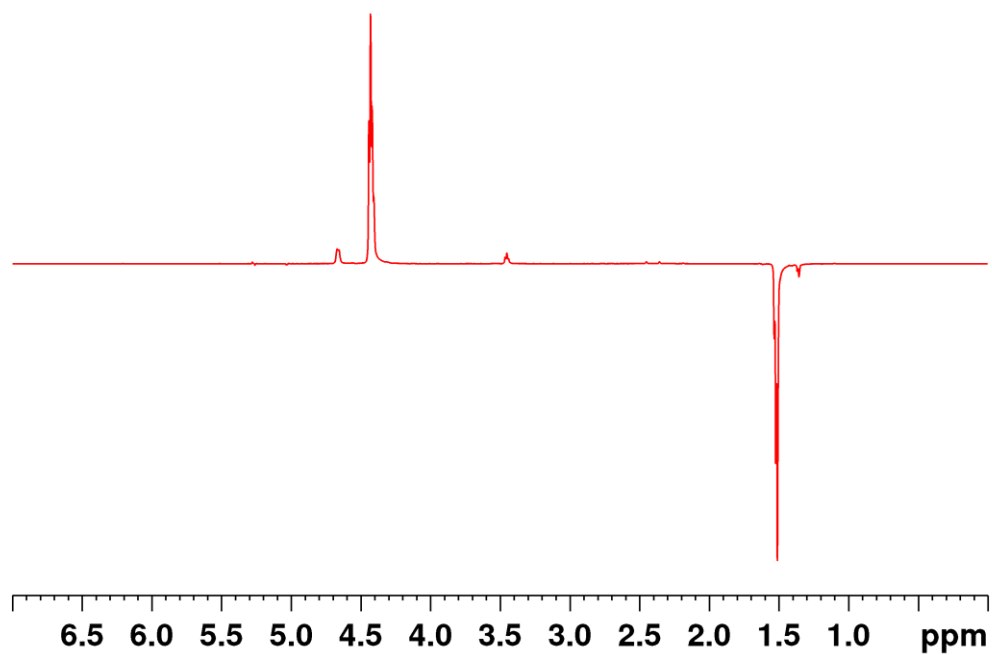


Figure S11. <sup>1</sup>H spectrum of a single scan of EA formation after para-H<sub>2</sub> bubbling.

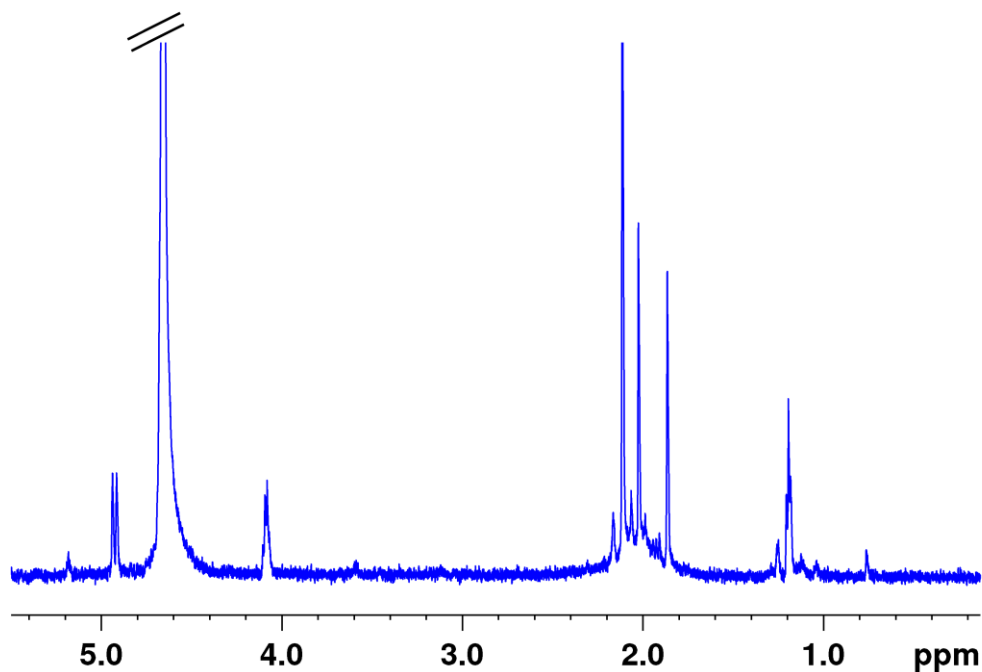


Figure S12.  $^1\text{H}$  spectrum of EA formation after reaching thermal equilibrium after 16 scans.

### Inversion Recovery

Longitudinal relaxation ( $T_1$ ) measurements of relevant  $^1\text{H}$ ,  $^{13}\text{C}$  and  $^{15}\text{N}$  nuclei were performed by inversion recovery. Inverse-gated proton decoupling was applied during  $^{13}\text{C}$  acquisition, and both proton and deuterium decoupling were applied during  $^{15}\text{N}$  acquisition for better sensitivity. Delay times were set to  $\geq 5 \times T_1$  in between measurements.

## S5 Polarization Calculations

### <sup>1</sup>H Polarization

<sup>1</sup>H signal enhancement values of all compounds investigated were determined by comparing intensities of hyperpolarized peaks in product <sup>1</sup>H spectra immediately after hydrogenation ( $S_{HP}$ ) to thermally polarized spectra after waiting  $\geq 3$  minutes ( $S_{therm}$ ). The number of scans required to accurately assess is accounted for in this calculation ( $n_{scans}$ ). The signal enhancement is then normalized to the number of protons contributing to thermal spectral peaks ( $\# \text{ } ^1H_{therm}$  and  $\# \text{ } ^1H_{HP}$ ) and multiplied by the <sup>1</sup>H thermal polarization at the appropriate field and temperature,  $P(^1H_{thermal})$ . This value is finally multiplied by 100 to provide % polarization:

$$\%P = \left( \frac{S_{HP}}{S_{therm} \times n_{scans}} \right) \times \left( \frac{\# \text{ } ^1H_{therm}}{\# \text{ } ^1H_{HP}} \right) \times P(^1H_{thermal}) \times 100$$

### <sup>13</sup>C and <sup>15</sup>N Polarization

<sup>13</sup>C and <sup>15</sup>N product peaks immediately following hydrogenation and transfer methods are directly compared to external reference (<sup>15</sup>N-urea for NETMA, 1-<sup>13</sup>C-pyruvate for HEP) or thermally polarized product spectra (EA). Hyperpolarized intensities are determined by integration ( $S_{HP}$ ) and compared to reference solutions measured with identical experimental calibrations using a single scan ( $S_{ref}$ ). The difference in their concentrations is then represented by multiplication of their concentration ratios ( $c_{ref}$  and  $c_{HP}$ ), followed by the thermal polarization of the nucleus at the relevant field and temperature ( $P(^{15}N_{therm} \text{ or } ^{13}C_{therm})$ ), and finally by 100 to report % polarization:

$$\%P = \left( \frac{S_{HP}}{S_{ref}} \right) \times \left( \frac{c_{ref}}{c_{HP}} \right) \times P(^{15}N_{therm} \text{ or } ^{13}C_{therm}) \times 100$$

## S6 References

- [1] J. McCormick, A. M. Grunfeld, Y. N. Ertas, A. N. Biswas, K. L. Marsh, S. Wagner, S. Glögler, L. S. Bouchard, *Anal. Chem.* **2017**, *89*, 7190–7194.
- [2] T. Futschek, M. Marsman, J. Hafner, *J. Phys. Condens. Matter* **2005**, *17*, 5927–5963.
- [3] R. V. A. N. Hardeveld, F. Hartog, *Surf. Sci.* **1969**, *15*, 189–230.